第33卷第1期
2014年2月

红外与毫米波学报
J. Infrared Millim. Waves

Vol. 33, No. 1
February, 2014

文章编号：1001－9014(2014)01－0055－07

DOI：10.3724/SP.J.1010.2014.00055

Simulation and design of a W-band third-harmonic gyrotron oscillator

SHI Shao-Hui[1,3,4], LIU Pu-Kun[2*], DU Chao-Hai[2], XU Shou-Xi[1], GENG Zhi-Hui[1], LI Zheng-Di[1,3], WANG Hu[1,3]

(1. Institute of Electronics, Chinese Academy of Sciences, Beijing 100190, China;
2. School of Electronics Engineering and Computer Science, Peking University, Beijing 100871, China;
3. University of Chinese Academy of Sciences, Beijing 100049, China;
4. Department of Physics, Shijiazhuang University, Shijiazhuang 050035, China)

Abstract: Some key issues associated with the interaction efficiency of a harmonic gyrotron oscillator operating in the millimeter wave regions were studied. Operating at the third-harmonic, the required magnetic field was reduced to 1.185 T for a 94 GHz gyrotron oscillator, which makes it possible to replace the superconducting magnet by a permanent magnet. A self-consistent code and a particle-in-cell(PIC) software were used to investigate the harmonic beam-wave interaction. The interplay between the cavity quality factor and interaction efficiency was revealed, and the dependence of both beam voltage and electron beam pitch factor on the coupling coefficient was also studied. Through carefully choosing operating mode, optimizing system parameters, and using linearly increased axial magnetic field, the output power of 95 kW and efficiency of 19.7% was achieved under accelerating voltage of 40 kV, beam current of 12 A, and transverse velocity spread of 3%. The efficiency can be further increased to 39.2% by utilizing a single stage depressed collector(SDC).

Key words: gyrotron; oscillator; W-band; third-harmonic

PACS: 84.40.Ik

W波段三次谐波回旋振荡管的模拟与设计

史少辉[1,3,4]，刘濮鲲[2*]，杜朝海[2]，徐寿喜[1]，耿志辉[1]，李铮迪[1,3]，王 虎[1,3]

(1. 中国科学院电子学研究所,北京 100190;2. 北京大学信息科学技术学院,北京 100871;
3. 中国科学院大学,北京 100049;4. 石家庄学院物理学系,河北 石家庄 050035)

摘要：研究了影响毫米波谐波回旋管互作用效率的多个因素，通过采用三次谐波工作，94 GHz回旋管的工作磁场降低到了1.185 T，使采用永磁体取代超导磁体成为可能.利用自洽非线性计算和粒子模拟研究了回旋振荡管的注-波互作用过程，发现了腔体品质因数与互作用效率的内在联系，研究了工作电压和电子注横纵速率比对耦合强度的影响，考虑了磁场渐变及电子注速度离散对互作用效率的影响，通过选择合理的工作模式和系统参数，当工作电压为40 kV、工作电流为12 A、电子注横向速度离散为3%时获得了95 kW的输出功率及19.7%的效率.当采用单级降压收集极后，效率可以进一步提高到39.2%.

关 键 词：回旋管;振荡器;W波段;三次谐波

中图分类号：TN129　　**文献标识码**：A

Received date: 2013-04-22, **revised date**: 2013-06-21　　**收稿日期**：2013-04-22，**修回日期**：2013-06-21

Foundation items: Supported by National Science Fund of China(11275206, 61072024, 61072026, 60971072, 11178016), and the Key Project of Natural Science Foundation of China under(60931001), and Foundation of Shijiazhuang University under(XJPT002).

Biography: Shi Shao-Hui(1983-), male, Shijiazhuang, Ph. D. Research area involves high power millimeter source and technology. E-mail: shishaohui-1983@163.com.

* **Corresponding author**: E-mail: pkliu@ieee.org.

Introduction

A gyrotron is a fast-wave device based on the electron cyclotron maser(ECM) instability, which is capable of delivering high-power radiation in the millimeter to terahertz wave regions[1-3]. At present, gyrotrons have been widely applied in the fields of electron cyclotron resonance heating(ECRH), electron cyclotron current drive (ECCD), dynamic nuclear polarization enhanced nuclear magnetic resonance (DNP-NMR), plasma diagnosis, weather monitoring, ceramic sintering, high-resolution radar, and so on[4-5].

The ECM principle brings a gyrotron with capability of generating strong radiation than normal vacuum electron devices(VEDs) in the same frequency ranges, and the required magnetic field strength approximately proportional to the radiation frequency, which means a superconducting magnet is unavoidable for a fundamental harmonic millimeter-wave gyrotron. In order to reduce the operating magnetic field strength in a gyrotron, the sth cyclotron harmonic operation was proposed, which reduce the magnetic field to 1/s of the fundamental scheme. Harmonic gyrotron experiments have been carried out all over the world to explore the advantage of low operating magnetic field. In Russia, several harmonic gyrotron experiments in THz range have been successfully carried out, including a 1.00 THz third-harmonic gyrotron oscillator[6], a 0.258 THz second-harmonic gyrotron oscillator[7], and a 0.4 THz third-harmonic gyrotron oscillator[8]. In Japan, a second-harmonic THz gyrotron oscillator was fabricated at University of Fukui(FU), the measured output frequency was 1.005 THz[9]. Besides, the FU has developed a series of THz gyrotron oscillators(FU CW series), many of which adopted harmonic operation scheme[10-11]. In America, a 16W continuous-wave(CW) output power was achieved for a 0.46 THz second-harmonic gyrotron oscillator at Massachusetts Institute of Technology (MIT)[12]. In China, a 0.42 THz second-harmonic gyrotron oscillator has been tested at the University of Electronic Science and Technology(UESTC), the output power of 4.4 kW was achieved utilizing a 8.1T pulsed magnet[13].

Although operating at a higher harmonic is with the advantage of low magnetic field strength, harmonic operation usually suffers from low beam-wave interaction efficiency because of mode competition and low coupling strength[14-19]. To explore solutions to increase the interaction efficiency is a critical problem to be solved before developing harmonic gyrotron oscillators. In this paper, a W-band third-harmonic gyrotron oscillator was investigated, much efforts were devoted to reveal the interplay between the system parameters, as a way to improve the interaction efficiency.

This paper is organized as follows. Section 1 gives the self-consistent nonlinear gyrotron theory which is used in the nonlinear code. Section 2 introduces the mode selection, cavity design and choosing of the beam parameters. Section 3 introduces the simulation results, which include optimization of the interaction cavity, the relation between the interaction efficiency and diffraction quality factor, the effect of magnetic field taper on interaction efficiency, and so on. In order to evaluate the engineering feasibility of realizing the harmonic gyrotron oscillator, a permanent magnet is designed, and a single stage depressed collector is introduced in section 4. Finally, a conclusion is made in section 5.

1 Nonlinear gyrotron theory

The process of beam-wave interaction can be described by the following three self-consistent equations[20-21]:

$$\frac{d\bar{u}_z}{dt} = 0 \quad , \tag{1}$$

$$\frac{d\bar{P}}{dt} + \frac{i}{\bar{u}_z}\left(\frac{\omega\gamma}{sc} - \frac{eB_0}{m_0 c}\right)\bar{P} = -\frac{i\eta_0\gamma C_{mn}k_{mn}f(z)}{2\bar{u}_z c^2} \times J_{m-s}(k_{mn}R_e)\frac{1}{(s-1)!}\left(\frac{k_{mn}\bar{p}^*}{2\Omega_0}\right)^{s-1}(ic)^{s-1} \quad , \tag{2}$$

$$\left(\frac{d^2}{dz^2} + \frac{\omega^2}{c^2} - k_{mn}^2\right)f(z) = -i\omega\mu_0\frac{I_0 C_{mn}k_{mn}}{2}\frac{1}{\bar{u}_z}\frac{1}{(s-1)!} J_{m-s}(k_{mn}R_e)\left(\frac{-ick_{mn}}{2\Omega_0}\right)^{s-1} \times \frac{1}{2\pi}\int_0^{2\pi}\bar{p}^s d(\omega t) \quad , \tag{3}$$

where $\bar{u}_z = u_z/c = \gamma v_z/c$ is normalized axial momentum, $\bar{u}_t = u_t/c = \gamma v_t/c$ is normalized transverse momentum, $f(z) = |f(z)|\exp(-i\psi(z))$ represents the axial electric field profile function, φ_e is the polar angle of guiding center, $\bar{P} = i\bar{u}_t\exp(-i\Lambda)$ represents normalized

momentum variable, $\Omega_0 = eB_0/m_0$ is the initial electron cyclotron frequency, C_{mn} is a normalization constant, $\eta_0 = |e|/m_0$ is the charge to rest mass ratio for an electron, $\Lambda = (\omega/s - \Omega)\tau - (\omega/s - 1)\varphi_e$ is slow time phase variable, and k_{mn} is transverse wave number.

Equation(1) is the function of axial momentum which is a constant because the axial force by the transverse magnetic was ignored in deriving Equation (1). Equation (2) is the electron motion function which illustrates the evolution of transverse momentum of the electron beam. Eq. (3) gives the evolution function of the electric field amplitude. Therefore, Eqs. (1 -3) constitute a set of self-consistent equations to describe the beam-wave interaction process.

Table 1　Parameters of $TE_{02}^{(3)}$ interaction system
表 1　$TE_{02}^{(3)}$ 互作用系统的工作参数

Cavity radius (mm)	3.56
Length of cutoff section L1(mm)	10
Length of middle section L2(mm)	42
Length of output section L3(mm)	15
Diffractive quality factor	7432
Ohmic quality factor	16525
Operating mode	TE_{02}
Harmonic number	3
Accelerating voltage(kV)	40
Beam current(A)	12
Magnetic field strength(T)	1.185
Pitch factor	1.5
Velocity spread	3%

2　Cold cavity considerations

Third-harmonic modes are relatively difficult to be excited because their coupling strength is weaker than fundamental and second-harmonic modes[19]. To solve this problem, a cavity with high diffractive quality factor Q_d is usually used. The axis symmetrical TE_{02} mode is employed as the operating mode to release the problem of strong ohmic loss inherent with high Q_d cavity. A three-section cylindrical cavity with a long middle section(L_2) was chosen as the interaction circuit, the cavity parameters are listed in Table. 1. Figure 1 shows the uncoupled dispersion curves for the operating and nearby modes, the beam-wave synchronism lines of the first 3 harmonics are also plotted under the magnetic field of 1.185 T.

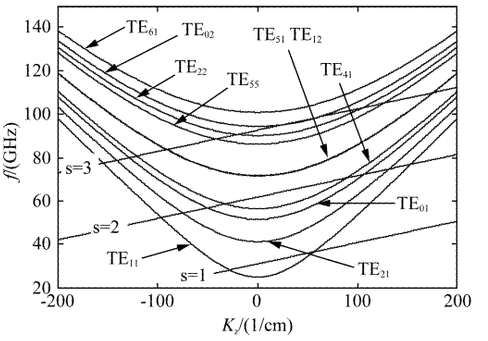

Fig. 1　The cold dispersion relations and beam-wave synchronism lines
图 1　冷腔色散曲线和注 - 波同步条件

According to the linear theory of gyrotron oscillator, the interaction strength between an electron beam and a TE_{mn} mode at the s-th cyclotron harmonic is given by the coupling coefficient[22]

$$H_{sm} = J_{m-s}^2(k_{mn}R_b)J'^2_s(k_{mn}R_L) \quad , \quad (4)$$

where s is the cyclotron harmonic number, k_{mn} is the transverse wave number, R_b and R_L are electron beam center radius and the Larmor radius, respectively.

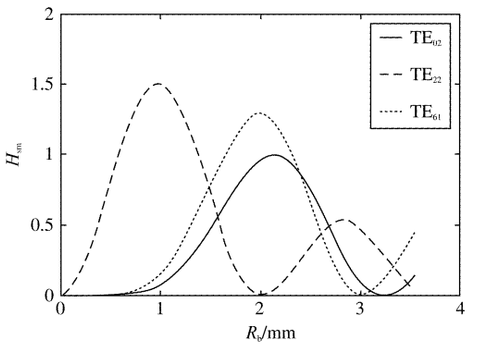

Fig. 2　Coupling coefficients of the operating mode along with nearby TE_{22} and TE_{61} modes
图 2　工作模式及近邻模式(TE_{22} 和 TE_{61})的耦合系数

The coupling coefficients for the operating mode and the nearby TE_{22} and TE_{61} modes are shown in Fig. 2. It shows that the coupling coefficient of TE_{02} mode reaches maximum at $R_b = 2.18$ mm. The second term at the right-hand side of Eq. (4) illustrates the relation between the accelerating voltage and coupling coefficients, to show the relation clearly, voltage coupling coefficient is introduced

$$H_{smu} = (v_\perp / c)^2 J'^2_s (k_{mn} R_L) \quad . \quad (5)$$

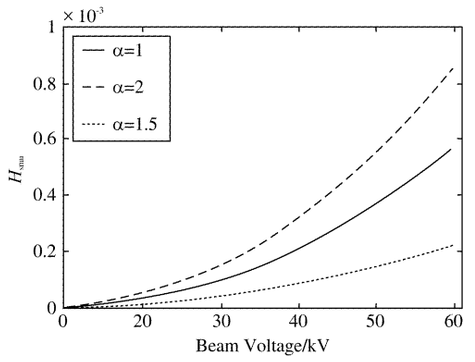

Fig. 3 Voltage coupling coefficients as a function of accelerating voltage for different velocity ratio
图3 电压耦合系数随电子注电压的变化情况

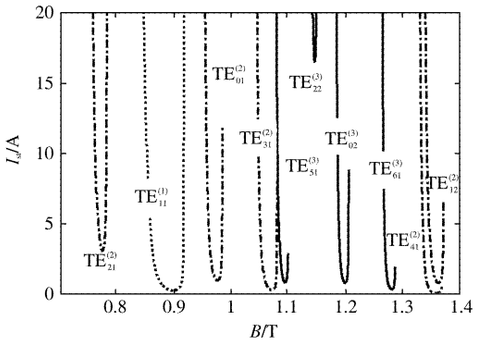

Fig. 4 Dependence of start oscillation current on magnetic field
图4 起振电流随工作磁场的变化关系

Figure 3 plots the dependence of voltage coupling coefficient on beam voltage and velocity ratio for magnetic field of 1.185 T. As shown in Fig. 3, the interaction strength increases with the beam voltage at fixed velocity ratio. Although high voltage will give strong interaction strength, a moderate voltage of 40 kV was chosen as the accelerating voltage for the interaction strength was strong enough as shown in section 3 (insulation requirement was also considered).

Figure 4 gives the starting current curves of all possible ten modes (see Fig. 1) at s = 1, 2, 3 for beam voltage U = 40 kV and velocity ratio α = 1.5. Here, starting currents of modes resonant with the third, second and first cyclotron harmonics are shown by solid, dash-dotted and dotted lines, respectively. It is clear that the operating TE_{02} mode is well separated from other competing modes. In order to operate at the hard excitation region, the magnetic field of 1.18T is chosen.

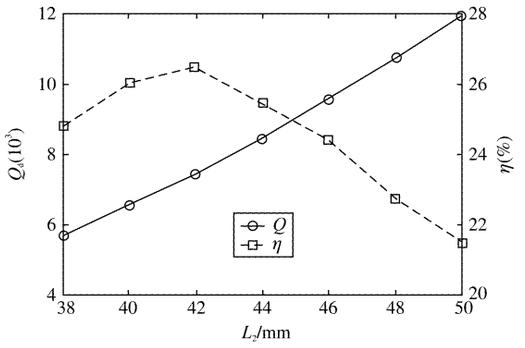

Fig. 5 Dependence of quality factor and interaction efficiency on the length of middle section
图5 品质因数和互作用效率与中间段长度的关系

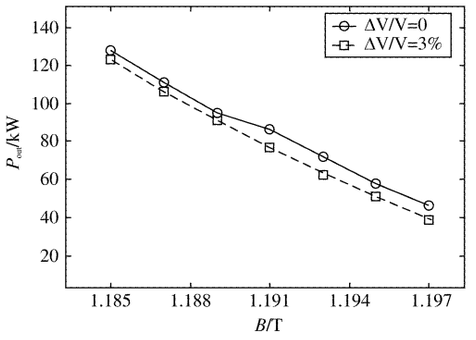

Fig. 6 Dependence of output power on magnetic field
图6 输出功率随工作磁场的变化情况

3 Beam-wave interactions

Because the diffractive quality factor Q_d is mainly decided by the length of the middle section (L_2), the dependence of Q_d and interaction efficiency on L_2 was studied by the nonlinear code and HFSS (see Fig. 5, parameters of the cavity are listed in Table 1). It can be seen from Fig. 5 that the diffractive quality factor increased quickly with L_2, however there is a maximum efficiency at L_2 = 42 mm. When L_2 is shorter than 42 mm, the interaction efficiency is lower because of the weaker RF field excited in the cavity. When L_2 is longer than 42mm, the interaction becomes too strong, which leads to "over-bunching", so the interaction efficiency is reduced, too. It can also be seen from Fig. 5 that, the diffractive quality factor for the maxi-

mum efficiency is 7432 which is approximately half of the ohmic quality factor 16525.

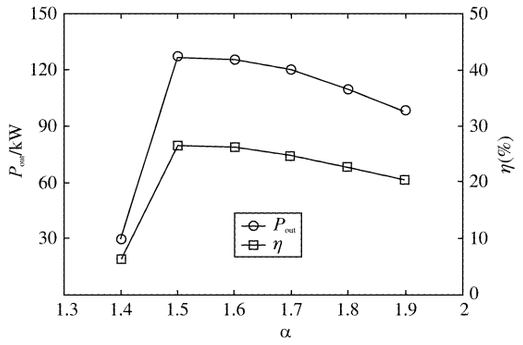

Fig. 7　Dependence of the output power and efficiency on the beam velocity ratio
图 7　输出功率和效率随电子注速度比的变化情况

Figure 6 gives the output power turning as a function of magnetic field for an ideal electron beam with the accelerating voltage of 40 kV and beam voltage current of 12A. It can be seen that the maximum output power of about 127 kW was achieved at 1.185 T. The output power for electron beam with 3% transverse velocity spread is also shown in Fig. 6. The reduction of output power and efficiency is very small, which shows the steady of the operating point to velocity spread.

The relation between interaction efficiency and the velocity ratio of electron beam was studied for accelerating voltage of 40 kV, beam current of 12A, and magnetic field of 1.185 T. As shown in Fig. 7, there is a maximum output power point at the velocity ratio of 1.5, and the corresponding output power and efficiency is 127 kW and 26%, respectively.

The start-up scenario of the operating mode simulated by the PIC software is showed in Fig. 8. The excitation time is about 250ns which is longer than the fundamental and second-harmonic gyrotron oscillators because of the lower coupling strength. The output power increases sharply between 250 ~ 320ns and then level off after 350ns with the maximum value of 127 kW. Fig. 9 plots the frequency spectrum of the RF field at the output port, the center frequency is 94 GHzV and it demonstrates no competition modes.

In order to enhance the interaction efficiency, we have studied the relation between magnetic field taper and interaction efficiency. The simulation showed that

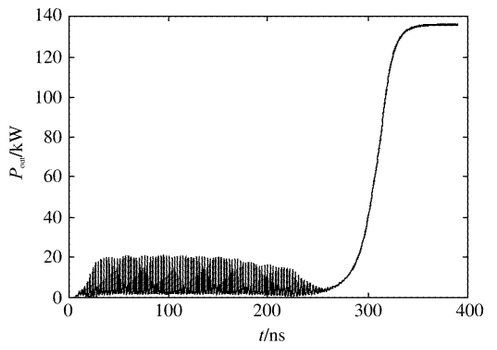

Fig. 8　Evolution of the output power at the output port
图 8　输出端口的输出功率随时间的变化

the interaction efficiency can be improved when up-tapered magnetic field was used in middle section of the cavity. The magnetic taper can be depicted by the following equation:

$$B(z) = B_{ave}\left(1 - \frac{1}{2}\Delta B/B_{ave} + \Delta B \times z/B_{ave}/L_{cav}\right) \quad .(6)$$

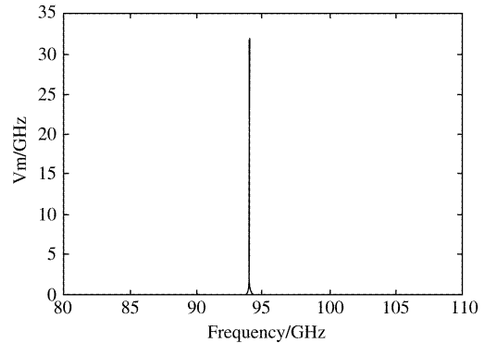

Fig. 9　Frequency spectrum at the output port
图 9　输出端的频谱分布

Figure 10 gives the output power and efficiency as a function of magnetic field taper, which shows that a small magnetic up-taper can enhance the output power evidently. The interaction efficiency reaches maximum at $\Delta B/B_{ave} = 1\%$, the corresponding power and efficiency is 138 kW and 28.5%, respectively (the corresponding output power and efficiency for the cavity with no magnetic taper is 127 kW and 26%, respectively).

4　Permanent magnet and depressed collector

The magnetic field strength for the W-band 3rd harmonic gyrotron is 1.185 T, which can be achieved by rare earth permanent magnet. In order to evaluate the

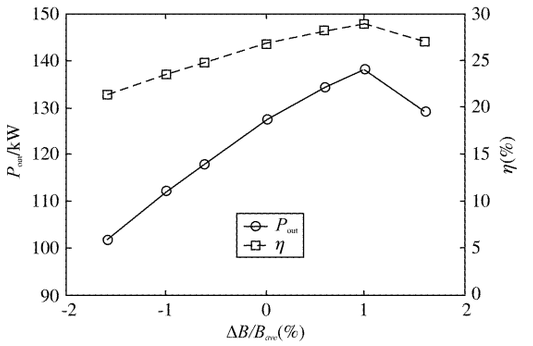

Fig. 10 Output power and interaction efficiency versus magnetic taper
图 10 输出功率和效率随磁场渐变的变化情况

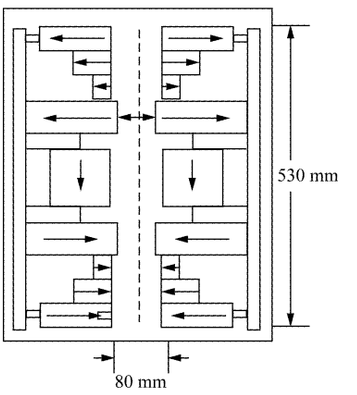

Fig. 11 Structure of the permanent magnet
图 11 永磁铁的结构图

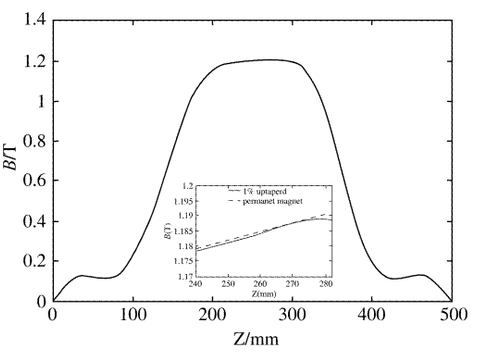

Fig. 12 The magnetic field intensity along the center axis
图 12 磁场强度随轴向坐标的变化关系

engineering feasibility of 3rd harmonic gyrotron based on permanent magnet, the software MAXWELL was used to design the magnet, and Nd-Fe-B was chosen as the permanent material. The magnet structure was carefully designed to generate an appropriate profile of magnetic field. The finished structure of the magnet is shown in Fig. 11, the arrow in the figure denotes the magnetization orientation. The material of the squares with no arrow is ferrite. The magnetic field profile is shown in Fig. 12, a 1% up-taper is designed in the interaction region. The difference between the designed and linear tapered magnetic field profile is very small which can be seen from the inset of Fig. 12. It should be noticed that further optimization was needed for the permanent magnet to satisfy the needs of special magnetron injection gun, and a coil was also needed to guarantee the stabilization of the magnetic field.

Unlike gyrotrons with low diffractive quality factors where losses are dominated by diffraction, the output power of gyrotrons with high Q_d is severely reduced by ohmic loss. In such a case, the output efficiency should be calculated by

$$\eta_{out} = \frac{p_{out}}{p_{in}} = \eta_{el} \times \eta_{RF} \quad , \quad (7)$$

where η_{el} is the electron efficiency, η_{RF} is RF efficiency which is the ratio of output power and the lost energy of electron beam, given by

$$\eta_{RF} = \frac{p_{out}}{p_{out} + p_{ohm}} = \frac{Q_{ohm}}{Q_d + Q_{ohm}} \quad , \quad (8)$$

Eq. (8) indicates that the RF efficiency will decrease with the increasing of diffractive quality factor. Substituting Q_d and Q_{ohm} into Eq. (8), the RF efficiency of 69% is obtained, which means that 31% of the power radiated by the electron beam will be dissipated on the cavity wall.

A gyrotron converts only the rotational energy into microwave energy, after beam-wave interaction, the rest energy of the electron beam will be dissipated in the collector. In order to recover the rest energy and enhance the overall efficiency, a single stage depressed collector is adopted. With a depressed collector, the overall efficiency of a gyrotron is given by

$$\eta_1 = \eta_{out} \frac{U_0}{U_0 - U_T} \quad , \quad (9)$$

where U_0 is the accelerating voltage of the electron beam, and U_T is the decelerating voltage of the collector. To avoid electron reflex from the collector, U_T must be chosen carefully. If the minimum energy of the electron beam leaving the interaction region is $eW_{\min}$,

then the decelerating voltage $U_T \leqslant W_{\min}$. Fig. 13 plots the energy distribution of the spent electron beam, and the minimum energy is about 22 keV, so we can set $U_T = 20$ kV which is smaller than the minimum energy of 22 keV to keep a safe margin. Using Eqs. (7) - (9), the overall output efficiency could be enhance from 19. 7% to 39. 2% when the collector was adopted.

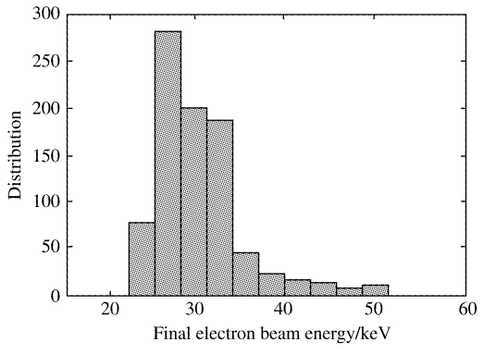

Fig. 13　Energy distribution of the spent electron beam
图 13　注 - 波互作用后的电子注能量分布

5　Conclusions

The paper presents investigation of the beam-wave interaction process of a third harmonic gyrotron oscillator using a self-consistent nonlinear code and a PIC simulation software. Investigation of linear theory shows that the beam-wave coupling strength can be improved by increasing the electron beam accelerating voltage and velocity ratio. It is found that the interaction efficiency achieves maximum when Q_d is approximately half of Q_{ohm}. The nonlinear simulation shows that the enhancement of 2. 5% efficiency is achieved utilizing a 1% axial linearly tapered magnetic field in the uniform section of the cavity. Based on the simulation results, a W-band third-harmonic gyrotron oscillator was optimized. Through carefully optimizing the cavity structure, beam parameters, tapered magnetic field profile, the gyrotron oscillator achieved output power of 95 kW and output efficiency of 19. 7%. A rare earth permanent magnet is specially designed to achieve magnetic field strength up to 1. 185 T to present the W-band 3rd harmonic gyrotron. Thus, this gyrotron oscillator is very suitable for W-band active denial nonlethal weapon system. This work is also useful for developing harmonic terahertz gyrotrons.

Acknowledgment

This work was supported in part by the National Science Fund of China under Contract Nos. 11275206, 61072024, 61072026, 60971072, and 11178016 and the Key Project of Natural Science Foundation of China under Grant 60931001, and Foundation of Shijiazhuang University under Grant XJPT002.

REFERENCES

[1] Chu K R. The electron cyclotron master, *Pre. Mod. Phys* [J]. 2004, **76**(2), 489 - 540.
[2] Kartikeyan M V, Borie E, Thumm M. Gyrotrons High-Power Microwave and Millimeter Wave Technology [M]. *Germany*, *Springer*, 2004.
[3] Nusinovich G S. Introduction to the Physics of Gyrotrons [M]. *Maryland*, *Johns Hopkins University Press*, 2004.
[4] Nitin Kumar, Udaybir Singh, Singh T. P., *et al.* A review on the applications of high power, high frequency microwave source: gyrotron. *J Fusion Energy*[J]. 2011, **30**: 257 - 276.
[5] Vladimir Bratman, Mikhail Glyavin, Toshitaka Idehara, *et al.* Review of subterahertz and terahertz gyrodevices at IAP RAS and FIR FU, *IEEE Trans Plasma Sci*[J]. 2009, **37**(1): 36 - 43.
[6] Bratman V L, Kalynov Yu K, Manuilov V N. Larg-orbit gyrotron operation in the terahertz frequency range, *Physical Review Letters*[J]. 2009, **102**, 245101.
[7] Zavolsky N A, Zapevalov V E, MAlygin O V, *et al.* Optimization of the cavity of a second- cyroharmonic continuous-wave gyrotron with an operating frequency of 258 GHzV, *Radiophysics and Quantum Electronics* [J]. 2009, **52**(5-6); 379 - 385.
[8] Mikhail Yu Glyavin, Alexey G. Luchinin, Vladimir N. Manuilov, *et al.* Design of a subterahertz, third-harmonic continuous-wave gyrotron, IEEE Trans. Plasma Sci [J]. 2008, **36**(3): 591 - 596.
[9] Idehara T, Tsuchiya H, Watanabe O, *et al.* The first experiment of a THz gyrotron with a pulse magnet, *International Journal of Infrared and Millimeter Waves* [J]. 2006, **27**(3): 319 - 331.
[10] Toshitaka Idehara, Kosuke Kosuga, La Agusu, *et al.* Gyrotron FU CW Ⅶ for 300 MHz and 600 MHz DNP-NMR spectroscopy, *J. Infrared Milli Terahz Waves*[J]. 2010, **31**: 763 - 774.
[11] Idehara T, Saito T, Ogawa I, *et al.* Development of Terahertz FU CW gyrotron series for DNP, *Appl. Magn. Reson* [J]. 2008, **34**: 265 - 275.
[12] Antonio C. Torrezan, Seong-Tae Han, *et al.* Continuous-wave operation of a frequency-tunable 460-GHz second-harmonic gyrotron for enhanced nuclear magnetic resonance, *IEEE Trans. Plasma Sci* [J]. 2010, **38**(6): 1150 - 1159.
[13] Fu Wenjie, Yan yang, Li xiaoyun, *et al.* Generating 0.42 THz radiation from a second harmonic gyrotron, *Chinese Science Bulletin*[J]. 2011, **56**(33): 3572 - 3574.

(下转第 105 页)

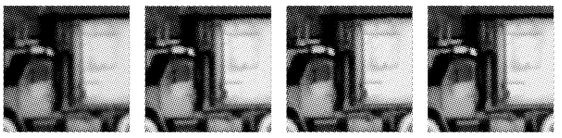

(a)　(b)　(c)　(d)

Fig. 11　Partially magnified images shown in Fig. 11: (a) BI; (b) Algorithm Ⅱ; (c) Algorithm Ⅰ; (d) Proposed algorithm

图 11　图 10 中的部分放大图像: (a) 双线性插值法; (b) 算法Ⅱ; (c) 算法Ⅰ; (d) 本文提出的算法

5　Conclusions

In this paper, a novel adaptive regularization method was proposed. The regularization term only penalizes the low-frequency components and protects the high-frequency which may represent edge. The penalty threshold is determined by a linear function. The regularization parameter is adaptively selected by a logarithmic function based on the ratio of fidelity term and regularization term. The experimental results show that the proposed method can preserve the edge well and obtain better results than the Gaussian MRF-based method and constant parameter method in both quantitative term and visual effects.

REFERENCES

[1] Wallach D, Lamare F, Roux C, *et al*. Biomedical Imaging: From Nano to Macro, [J]. *IEEE International Symposium on*, **2009**: 931 - 934.

[2] Chan J-W, Ma J, Kempeneers P, *et al*. Superresolution enhancement of hyperspectral CHRIS/Proba images with a thin-plate spline nonrigid transform model [J]. *Geoscience and Remote Sensing, IEEE Transactions on*, 2010, **48**(6): 2569 - 2579.

[3] Huang T S, Tsay R Y. Advances in Computer Vision and Image Processing, [J]. 1984, **1**(2): 317 - 339.

[4] Park S C, Park M K, Kang M G. Super-resolution image reconstruction: a technical overview [J]. *Signal Processing Magazine, IEEE*, 2003, **20**(3): 21 - 36.

[5] Qin F-q, He X-h, Chen W-l, *et al*. Video superresolution reconstruction based on subpixel registration and iterative back projection [J]. *Journal of Electronic Imaging*, 2009, **18**(1): 013007 - 013007 - 013011.

[6] Estrela V V, Galatsanos N P. Image Processing, 1998. ICIP 98. Proceedings [C]. 1998 *International Conference on*, 1998, **2**: 200 - 203.

[7] Bose N K, Lertrattanapanich S, Koo J. Circuits and Systems, 2001. ISCAS 2001 [C]. *The* 2001 *IEEE International Symposium on*, 2001, **2**: 433 - 436.

[8] Krawczyk-StańDo D, Rudnicki M. Regularization parameter selection in discrete ill-posed problems—the use of the U-curve [J]. *International Journal of Applied Mathematics and Computer Science*, 2007, **17**(2): 157 - 164.

[9] Panagiotopoulou A, Anastassopoulos V. Regularized super-resolution image reconstruction employing robust error norms [J]. *Optical Engineering*, 2009, **48**(11): 117004 - 117004 - 117014.

(上接 61 页)

[14] YUAN Xue-Song, LAN Ying, MA Chun-Yan, *et al*. Theoretical study on a 0.6 THz third harmonic gyrotron, *Phys. Plasmas* [J], 2011, **18**: 103115.

[15] GENG Zhi-Hui, LIU Pu-Kun, SU Yi-Nong, *et al*. Design of a Ka band 35 kW CW low-voltage harmonic gyrotron [J], *Int J. Infrared Millim. Waves*, 2010, **31**(1): 41 - 47.

[16] CAO Xiao-Qin, LIU Pu-Kun. Self-consistend nonlinear computation of a 28 GHzV gyrotron at the second harmonic. [J]. *J. Infrared Millim. Waves* (曹晓琴, 刘濮鲲. 28 GHzV二次谐波回旋振荡管的自洽非线性计算. **红外与毫米波学报**)2005, **24**(4): 317 - 320.

[17] YUAN Xue-Song, YAN Yang, FU Wen-Jie, *et al*. Multimode high harmonic operation in a terahertz gyrotron. [J]. *J. Jnfrared Millim. Waves* (袁学松, 鄢扬, 傅文杰, 等, 高次谐波太赫兹回旋管的多模工作. **红外与毫米波学报**)2012, **31**(4): 342 - 347.

[18] Huang Yong, Li Hongfu, Du Pingzhong, *et al*. Third-harmonic complex cavity gyrotron self-consistent nonlinear analysis, *IEEE Trans. Plasma Sci* [J]. 1997, **25**(6): 1406 - 1411.

[19] Du Chao-Hai, Liu Pu-Kun . Beam-wave coupling strength analysis in a gyrotron traveling-wave amplifier, *J Infrared Milli Terahz Waves* [J]. 2010, **31**: 714 - 723.

[20] Liu P-K, Borie E, Kartikeyan M V. Design of a 24 GHzV, 25-50 kW technology gyrotron operating at the second harmonic, Int. *J. Infrared and Millimeter Waves* [J]. 2000, **21**(12): 1917 - 1943.

[21] Fliflet A W, Read M E, Chu K R, *et al*. A self- consistent field theory for gyrotron oscillator: application to a low Q gyromonotron, Int. *J. Electronics* [J]. 1983, **53**(6): 505 - 521.

[22] Chu K R. Theory of electron cyclotron maser interaction in a cavity at the harmonic frequencies, *Phys. Fluids* [J]. 1978, **21**(12): 2354 - 2364.